**FERMILAB-PUB-09-663-APC**

January 28, 2010

# MUON COLLIDERS AND NEUTRINO FACTORIES

Steve Geer[1]

Fermi National Accelerator Laboratory, PO Box 500, Batavia, IL 60510

email: sgeer@fnal.gov

Keywords: accelerators, storage rings, high energy colliders, muon sources

**ABSTRACT**

Over the last decade there has been significant progress in developing the concepts and technologies needed to produce, capture and accelerate $O(10^{21})$ muons/year. This development prepares the way for a new type of neutrino source (Neutrino Factory) and a new type of very high energy lepton-antilepton collider (Muon Collider). This article reviews the motivation, design and R&D for Neutrino Factories and Muon Colliders.

## 1. INTRODUCTION

The muon, which can be thought of as a heavy electron, lives just long enough ($\tau_0$=2μs) to enable it to be accelerated to high energy before it decays into an electron, a muon-type neutrino and an electron-type antineutrino ($\mu^- \rightarrow e^- \nu_\mu \bar{\nu}_e$). Over the last decade there has been significant progress in developing the concepts and technologies needed to produce, capture and accelerate $O(10^{21})$ muons/year. This prepares the way for (i) a Neutrino Factory (NF) in which high energy muons decay within the straight sections of a storage ring to produce a beam of neutrinos and anti-neutrinos, and (ii) a Muon Collider (MC) in which $\mu^+$ and $\mu^-$ are brought to collision in a storage ring.

Muon Colliders were proposed by Budker [1] in 1969. The concept was developed in the 1970's and 1980's by Skrinsky et al. [2] and Neuffer [3]. In the early 1990's it was realized that it might be possible to build a MC with a center-of-mass energy (√s) of a few TeV and a luminosity in the $10^{34}$ – $10^{35}$ $cm^{-2}s^{-1}$ range [4,5], and that a multi-TeV lepton collider with this luminosity is likely to be needed to fully explore the physics responsible for electroweak symmetry breaking. A MC R&D collaboration was formed in 1997. The NF concept was proposed [6] in November 1997, at a time when the discovery [7] that the three known types (flavor) of neutrino ($\nu_e, \nu_\mu, \nu_\tau$) can change their flavor as they propagate through space (neutrino oscillations [8]), was providing us with a first glimpse of physics beyond the Standard Model. Since NFs and MCs require similar muon sources, the U.S. MC Collaboration embraced NF R&D and became the NF and MC Collaboration (NFMCC). In addition, studies in the U.S. [9,10], Europe [11] and

Japan [12] consolidated the physics case, explored alternative designs, and ultimately led to a globalization of NF R&D.

## 2. NEUTRINO FACTORIES: CONCEPT AND BEAM PROPERTIES?

Conventional neutrino beams are produced from charged pions decaying in a long channel. If $\pi^+(\pi^-)$ are selected, the resulting beam consists of $\nu_\mu$ $(\bar{\nu}_\mu)$ from $\pi^+ \to \mu^+\nu_\mu$ $(\pi^- \to \mu^-\bar{\nu}_\mu)$ decays. To fully explore neutrino oscillations it is desirable to also have $\nu_e$ $(\bar{\nu}_e)$ beams by, for example, exploiting the decays $\mu^+ \to e^+\nu_e\bar{\nu}_\mu$ $(\mu^- \to e^-\nu_\mu\bar{\nu}_e)$. However, since $\mu^\pm$ live 100 times longer than $\pi^\pm$, a linear muon decay channel would need to be tens of kilometers long. To overcome this difficulty, in a NF the muons are injected into a storage ring with long straight sections. The fraction *f* of muons that decay in the straight section is given by the ratio of the straight section length to ring circumference. In NF designs typically *f* ~ 0.3.

A NF is shown schematically in Fig. 1a. It consists of:

i) A high-power multi-GeV proton source.

ii) A target within a high-field solenoid followed by a $\pi^\pm$ decay channel.

iii) A system of rf cavities that captures the daughter muons longitudinally into a bunch train, and then applies a time-dependent acceleration that increases the energy of the slower (low energy) bunches and decreases the energy of the faster (high energy) bunches (phase rotation).

iv) A cooling channel that reduces the transverse phase space occupied by the beam, so that it fits within the acceptance of the first acceleration stages.

v) An acceleration scheme that accelerates the muons.

vi) A storage ring with at least one long straight section that points through the earth to a distant detector.

End-to-end NF simulations show that if the primary proton beam power is ~4MW there will be up to $O(10^{21})$ muons per year decaying in the beam-forming straight section. In a near detector the resulting event rates would be very large. For example, a few tens of meters from the end of a 50 GeV NF, $10^{21}$ muon decays would result in $O(10^7)$ neutrino events/g/cm$^2$. Perhaps even more exciting, in a very distant detector the event rates (Table 1) are sufficient to probe neutrino flavor transition probabilities down to $O(10^{-4} - 10^{-5})$.

In addition, since muon decays are well understood, a NF offers low systematic uncertainties on beam fluxes and spectra. In the muon rest-frame the distribution of energies and angles is given by:

$$\frac{d^2 N_{\nu_\mu}}{dx d\Omega_{c.m.}} \propto \frac{2x^2}{4\pi}\left[(3-2x)+(1-2x)P_\mu \cos\theta_{c.m.}\right],$$

$$\frac{d^2 N_{\bar{\nu}_e}}{dx d\Omega_{c.m.}} \propto \frac{12x^2}{4\pi}\left[(1-x)+(1-x)P_\mu \cos\theta_{c.m.}\right],$$

where $x \equiv 2E_\nu / m_\mu$ , $\theta_{c.m.}$ is the angle between the neutrino momentum vector and muon spin direction, and $P_\mu$ is the average muon polarization along the beam direction. The corresponding $\bar{\nu}_\mu$ and $\nu_e$ distributions for $\mu^+$ decay are obtained by changing $P_\mu \to -P_\mu$. In the forward direction ($\cos\theta_{lab} \approx 1$) the maximum $E_\nu$ in the laboratory frame $E_{\max} = \gamma[1+\beta\cos\theta_{c.m.}]m_\mu/2$, and:

$$\frac{d^2N_{\nu_\mu}}{dxd\Omega_{lab}} \propto \frac{1}{\gamma^2(1-\beta\cos\theta_{lab})^2}\frac{2x^2}{4\pi}\left[(3-2x)+(1-2x)P_\mu\cos\theta_{c.m.}\right],$$

$$\frac{d^2N_{\bar{\nu}_e}}{dxd\Omega_{lab}} \propto \frac{1}{\gamma^2(1-\beta\cos\theta_{lab})^2}\frac{12x^2}{4\pi}\left[(1-x)+(1-x)P_\mu\cos\theta_{c.m.}\right].$$

The spectrum of interactions in a long baseline experiment is given by the convolution of these distributions with the energy dependent cross-sections. If $E_\nu >$ ~10 GeV the cross-sections are dominated by deep inelastic scattering and proportional to $E_\nu$. In principle polarization can be used to modify the spectra, although it is difficult to achieve high polarization at the end of the NF muon source [13].

Precisely known fluxes and spectra provide an advantage compared to conventional neutrino beams, but the real NF advantage comes from the $\nu_e$ and $\bar{\nu}_e$ in the beams since the transitions $\nu_e \leftrightarrow \nu_\mu$ and $\bar{\nu}_e \leftrightarrow \bar{\nu}_\mu$ are expected to play a special role in future measurements. In a conventional beam the initial flavor is $\nu_\mu$ and experiments must search for $\nu_\mu \to \nu_e$ transitions. The experimental sensitivity is eventually limited by a small but annoying $\nu_e$ component in the initial beam and by backgrounds in which $\pi^0$s

from $\nu_\mu$ interactions are misidentified as electrons, and hence fake $\nu_e$ interactions. This makes it difficult to probe oscillation probabilities below $O(10^{-2})$. However, a NF experiment can search for $\nu_\mu$ appearance from $\nu_e \to \nu_\mu$ transitions by looking for a "wrong-sign muon [6]", i.e. a muon of opposite sign to the muons stored in the NF. It is straightforward to suppress backgrounds down to $\leq O(10^{-4})$ of the total event rate [9].

The NF detector is typically assumed to be a magnetized iron-scintillator sampling calorimeter of the type used by the MINOS experiment [14], but with finer sampling. This detector-type is well suited for identifying wrong-sign muons provided the muon penetrates well beyond any accompanying hadronic shower. In practice this means a minimum energy $E_\mu^{\min} \sim 4$ GeV, and hence an effective threshold on $E_\nu$ of ~10 GeV, and a minimum NF energy of ~20 GeV. If a lower energy NF is desired it will be necessary to reduce $E_\mu^{\min}$ by using, for example, a detector made from low-Z materials. Until recently, magnetizing the very large volume needed for a low-Z NF detector was thought to be prohibitively expensive. However, an idea has emerged in which the cost-driving cryostat needed for the detector superconducting solenoid is eliminated by shrinking the cryostat around the conductor. The resulting "superconducting transmission line" is then wound to form a large solenoid. Initial simulations have shown that a fully active scintillator detector in a 0.5T solenoid would be able to measure the muon sign for neutrino interactions down to ~500 MeV, facilitating NFs with energies of a few GeV [15].

## 3. NEUTRINO FACTORIES: PHYSICS

The discovery that neutrinos have masses and that neutrino flavors mix as they propagate through space has revolutionized our understanding of the nature of neutrinos and their role in the Universe. Although much has already been learnt about neutrino oscillations, many questions remain unanswered. Before considering these open questions, it is useful to introduce the phenomenological framework that describes three-flavor mixing [16]. The mass eigenstates ($\nu_1$,$\nu_2$,$\nu_3$) are related to the flavor eigenstates ($\nu_e$, $\nu_\mu$, $\nu_\tau$) by a 3×3 unitary matrix $U$, which can be parameterized using 3 mixing angles ($\theta_{12}$, $\theta_{23}$, $\theta_{13}$) and one complex phase ($\delta$):

$$\begin{pmatrix} \nu_e \\ \nu_\mu \\ \nu_\tau \end{pmatrix} = \begin{pmatrix} c_{13}c_{12} & c_{13}s_{12} & s_{13}e^{-i\delta} \\ -c_{23}s_{12} - s_{13}s_{23}c_{12}e^{i\delta} & c_{23}c_{12} - s_{13}s_{23}s_{12}e^{i\delta} & c_{13}s_{23} \\ s_{23}s_{12} - s_{13}c_{23}c_{12}e^{i\delta} & -s_{23}c_{12} - s_{13}c_{23}s_{12}e^{i\delta} & c_{13}c_{23} \end{pmatrix} \begin{pmatrix} \nu_1 \\ \nu_2 \\ \nu_3 \end{pmatrix}$$

where the $s_{ij}$ and $c_{ij}$ denote respectively $\sin\theta_{ij}$ and $\cos\theta_{ij}$. Neutrino oscillation measurements have established that:

$$U \approx \begin{pmatrix} 0.8 & 0.5 & ? \\ 0.4 & 0.6 & 0.7 \\ 0.4 & 0.6 & 0.7 \end{pmatrix}.$$

We have only an upper limit of $\theta_{13}$ and no knowledge of $\delta$, and hence little knowledge of $U_{13}$ except that its magnitude is small.

Neutrino oscillations are driven by splittings between the mass eigenstates. The evolution of a neutrino beam as it propagates through matter is given by [17]:

$$i\frac{d\nu_\alpha}{dt} = \sum_\beta \frac{1}{2E_\nu}\left[\Delta m_{31}^2 U_{\alpha 3}U_{\beta 3}^* + \Delta m_{21}^2 U_{\alpha 2}U_{\beta 2}^* + A\delta_{\alpha e}\delta_{\beta e}\right]\nu_\beta$$

where $\Delta m_{ij}^2 = m_i^2 - m_j^2$, and $A/(2E_\nu)$ is the amplitude for coherent forward Charged Current scattering of $\nu_e$ on electrons. In matter of density $\rho(\text{g/cm}^3)$ and electron fraction $Y_e$, $A = 2\sqrt{2}G_F N_e E_\nu = 1.52\times 10^{-4}\,\text{eV}^2\, Y_e\rho\, E_\nu(\text{GeV})$. Oscillation measurements have already determined $\Delta m_{21}^2$ and the magnitude (but not the sign of) $\Delta m_{31}^2$ .

The evolution equation can be solved numerically for a given matter profile to yield the probability $P_{\alpha\beta}$ that a neutrino of energy $E_\nu$ and initial flavor $\alpha$ will "oscillate" into a neutrino of flavor $\beta$ as it travels a distance $L$. For long baseline experiments $P_{\alpha\beta}$ can be expanded in the "hierarchy parameter" $\eta \equiv \Delta m_{21}^2/\Delta m_{31}^2$ and the small mixing angle parameter $s \equiv \sin 2\theta_{13}$. Keeping terms up to the 2nd order [18]:

$$P_{e\mu} \approx s^2 \sin^2\theta_{23}\frac{\sin^2\left[\left(1-\hat{A}\right)\Delta\right]}{\left(1-\hat{A}\right)^2} \pm \eta\, s\xi \sin\delta \sin\Delta \frac{\sin\left(\hat{A}\delta\right)}{\hat{A}}\frac{\sin\left[\left(1-\hat{A}\right)\Delta\right]}{\left(1-\hat{A}\right)}$$
$$+\ \eta\, s\xi\cos\delta\cos\Delta\frac{\sin\left(\hat{A}\delta\right)}{\hat{A}}\frac{\sin\left[\left(1-\hat{A}\right)\Delta\right]}{\left(1-\hat{A}\right)} + \eta^2\cos^2\theta_{23}\sin^2 2\theta_{12}\frac{\sin^2\left(\hat{A}\delta\right)}{\hat{A}^2}$$

where the sign of the 2nd term is + (–) for $\nu_\mu \to \nu_e$ ($\nu_e \to \nu_\mu$) and $\Delta \equiv \Delta m_{31}^2 L/(4E_\nu)$, $\xi \equiv \cos\theta_{13}\sin 2\theta_{12}\sin 2\theta_{23}$, $\hat{A} \equiv \pm A/\Delta m_{31}^2$. For neutrinos (antineutrinos) the sign of $\hat{A}$ is the same as (opposite to) the sign of $\Delta m_{31}^2$. Measuring $P_{e\mu}$ as a function of $L$ and $E_\nu$

can distinguish between the 4 terms, and enable all the oscillation parameters to be determined.

Given our present knowledge, the outstanding questions that can be addressed by neutrino oscillation measurements are: (i) What is the value of $\theta_{13}$, the mixing angle between first- and third-generation neutrinos? (ii) Do neutrino oscillations violate the symmetry CP ($\sin\delta \neq 0$)? If so, how can neutrino CP violation (CPV) drive a matter-antimatter asymmetry among leptons in the early universe (leptogenesis)? (iii) What does the pattern of neutrino masses look like? Are neutrino masses ordered in the same way as quark masses, or with the opposite hierarchy (what is the sign of $\Delta m^2_{31}$)? (iv) Are the neutrino mixing parameters in some way related to the quark mixing parameters, and if so, what clues does this give us about quark-lepton unification?

A series of studies [9,11,12,19] have explored the ability of NF experiments to establish a non-zero $\theta_{13}$, determine the mass hierarchy, and observe CPV. The sensitivity depends upon $\sin^2 2\theta_{13}$ and $\delta$. In Fig. 2 the simulated sensitivity for a 25 GeV NF is compared with corresponding sensitivities at various candidate future conventional beam facilities. The NF would extend the "reach" in $\sin^2 2\theta_{13}$–space by more than an order of magnitude. If $\sin^2 2\theta_{13} < O(0.01)$ the NF is the facility of choice.

If $\sin^2 2\theta_{13}$ is large (>0.02, say) conventional neutrino beam experiments should be able to measure $\theta_{13}$, determine the mass hierarchy, and perhaps provide the first evidence for

CPV. The experimental program must then focus on precision measurements that test the phenomenological framework, discriminate between competing theories, and provide clues about quark-lepton unification. Initial studies have shown that a 4 GeV NF [15] might yield good precision if $\theta_{13}$ is large (Fig. 3). The precision is likely to be limited by statistics and, since event rate is proportional to target mass, by the mass of the largest affordable detector.

## 4. NEUTRINO FACTORIES: DESIGN AND R&D

Over the last decade NF R&D has been advanced by a series of design and simulation studies complemented by component development and experimental tests. In the U.S. the studies [10,20,21] established viability, defined an initial R&D program, and produced a first NF cost estimate. The later studies improved the design to increase performance and reduce cost. During this period NF R&D also became "internationalized". In 2006 the International Scoping Study (ISS), hosted by RAL in the U.K., produced physics [19], accelerator [22], and detector [23] reports.

### 4.1 Proton Beam and Target

At the NF front-end the proton source must deliver short high-intensity multi-GeV bunches onto a target. The ISS baseline parameters are:

(i) Proton energy $5 < E_P < 10$ GeV, chosen to maximize $\pi^{\pm}$ production at fixed beam power. Note that some proponents favor $E_P > 10$ GeV to ease the task of creating short high intensity bunches.

(ii) Bunch length $\sigma_t$ < 3ns, needed because the downstream phase rotation channel requires initially short muon bunches.

(iii) Beam power = 4MW. This is considered to be within reach for the next generation of multi-GeV proton sources and/or their upgrades.

(iv) A liquid Hg-jet target injected into a 20T solenoid. A high-Z target is chosen to maximize $\pi^{\pm}$ production. The 20T solenoid radially confines essentially all $\pi^{\pm}$ coming from the target. The Hg-jet choice avoids the shock and radiation damage related target-lifetime issues that arise in a solid target. A system of solenoids downstream of the target matches the 20T solenoid into a larger bore 2T decay channel.

Early on in the studies, to establish the viability of this scheme, two critical steps were identified: (a) establish a viable design for a multi-MW proton source with the required characteristics, and (b) conduct a proof-of-principle demonstration of the target technology.

Multi-GeV multi-MW proton source designs are now being developed at a number of laboratories around the World, motivated by a broad range of interests which include, for example, high-intensity convention neutrino beams. Proton source R&D is being pursued within this broader context. We can anticipate that at least one viable design for a NF-class proton source will exist within a few years.

Target R&D has also advanced in recent years, and has culminated in the Mercury Intense Target experiment (MERIT [24]) which has successfully demonstrated a Hg-jet injected into a 15T solenoid and hit by a suitably intense beam from the CERN PS. The jet was viewed by high speed cameras (Fig. 4) which enabled measurement of (i) the time before the jet was disrupted, (ii) the velocity of jet fragments after disruption, (iii) the length of the jet segment disrupted, and (iv) the time before the jet re-established itself. Preliminary results have been encouraging, and suggest this technology could support beam powers in excess of 4MW.

### 4.2 RF in Magnetic Channels

The bunching, phase rotation, and cooling channel designs require high gradient normal conducting rf cavities operating in a magnetic channel. The initially preferred design exploited the penetrating nature of muons by using cavities in which the normally open rf cells are closed with thin conducting windows. At fixed peak power this doubles the effective accelerating gradient, and hence halves the required number of rf power sources. Thin beryllium windows for this purpose have been demonstrated in an 805 MHz test cavity. However, tests have shown that when this type of cavity is operated within a multi-Tesla co-axial solenoid the maximum rf gradient that can be achieved before breakdown is significantly reduced. It is possible that, with further R&D, surface treatments can be found to mitigate this effect. However, other solutions have also been proposed including:

(i) Using cavities filled with high pressure hydrogen gas [25]. An 805 MHz cell has been built and tested in a high field solenoid. No appreciable degradation of performance was observed with increasing magnetic field. In the coming months this technology will be tested in the presence of an intensely ionizing beam. It is possible that the ionization created in the cavity will limit its performance.

(ii) Using "magnetically insulated" cavities [26]. The magnetic field is designed so that it is parallel to surfaces where the rf gradients are maximum. This is expected to prevent energetic electrons from hitting these surfaces and causing problems.

(iii) Designing cooling channels in which the cavities are in regions of low magnetic field. This is not a preferred solution since it will mean longer less efficient channels.

Within the next couple of years the ongoing R&D is expected to determine which of these options are viable.

### 4.3 Bunching, Phase Rotation and Cooling

At the end of the decay channel the daughter muons have drifted some tens of meters, resulting in a time-energy correlation with the high-energy particles leading the low-energy particles. The decay channel is followed by a buncher section that uses rf cavities to form the beam into a bunch train, and a phase-energy rotating section that decelerates the early-rf-phase high energy bunches and accelerates the late-rf-phase low energy

bunches, so that each bunch has the same mean energy. Present designs deliver a bunch train that is 50m long, captured within a 2T solenoid channel.

The buncher parameters are determined by considering reference particles (1, 2) with velocities $\beta_1$ and $\beta_2$. The rf voltages are increased along the channel, with frequencies $f_{rf}$ and phases set to place 1 and 2 at the center of bunches. This can be accomplished if the rf wavelength $\lambda_{rf}$ increases along the buncher [27]:

$$N_B \lambda_{rf}(s) = N_B \frac{c}{f_{rf}(s)} = s\left(\frac{1}{\beta_2} - \frac{1}{\beta_1}\right)$$

where s is the total distance from the target and $N_B$ is an integer. In the present design, at the end of the channel all bunches have a mean momentum ~230 MeV/c, with $\mu^+$ and $\mu^-$ bunches interleaved within the rf cycle. The reduction in the overall energy spread effectively increases the number of useful muons by about a factor of 4 (Fig. 5).

The number of muons accepted by the downstream accelerators can be further increased by reducing the two-dimensional phase-space-area (emittance) in each transverse direction ($\varepsilon_x$ and $\varepsilon_y$) by a factor of a few. This can be accomplished using "ionization cooling [28]" in which the muons lose energy by ionization as they pass through an absorber. This reduces their momenta in the longitudinal- and transverse-directions. An rf cavity then replaces the lost energy by reaccelerating in the longitudinal direction. After repeating the process many times, the transverse momenta (and transverse emittances) are reduced. The rate at which the normalized transverse emittance $\varepsilon_{xN} = \beta\gamma\ \varepsilon_x$ changes as

muons with energy $E_\mu$ (GeV) lose energy by ionization loss $dE_\mu / ds$ within material with radiation length $L_R$ is given by:

$$\frac{d\varepsilon_{Nx}}{ds} = -\frac{dE_\mu}{ds}\frac{\varepsilon_{Nx}}{E_\mu} + \frac{\beta_\perp (0.014)^2}{2E_\mu m_\mu L_R} \ ,$$

where $\beta_\perp$ is the "betatron function" which characterizes the focusing strength at the absorber. The second term describes heating due to scattering in the absorber which ultimately limits the cooling process. To minimize the impact of scattering it is desirable to use a low Z (high $L_R$) absorber (e.g. liquid hydrogen or LiH) and to focus the muons strongly (small $\beta_\perp$) so that the focusing angles are much larger than typical scattering angles. The present baseline cooling channel design consists of a sequence of LiH absorbers and 201 MHz rf cavities within a lattice of solenoids that provide the required focusing (Fig. 6). Simulations show that the cooling channel increases the number of useful muons by about a factor of 2 (Fig. 5).

To provide a proof-of-principle demonstration, the international Muon Ionization Cooling Experiment (MICE [29]) at RAL is preparing to test an ionization cooling channel cell in a muon beam (Fig. 7). MICE will measure the response of individual muons to the cell as a function of the incident muon parameters (momentum, position, direction) and the various channel parameters (absorber type, magnetic fields, rf parameters). The initial phase of the experiment, which establishes the muon beam and measurement systems, has begun. It is anticipated that MICE will be completed by 2011-2012.

### 4.4 Acceleration and Storage

Since muons are short-lived, acceleration must occur at high average gradient. The accelerator must also accommodate the phase-space occupied by the beam. Typically the normalized transverse emittances are $\varepsilon_{Nx} \approx \varepsilon_{Ny} \sim 4\,\text{mm-rad}$, longitudinal emittance $\varepsilon_L \sim 36\,\text{mm}$, momentum spread $\sigma_{\Delta p/p} \sim 0.1$, and bunch length $\sigma_Z \sim 0.16\,\text{m}$. The need for large transverse and longitudinal acceptances favors using low frequency rf. Acceleration systems have been designed assuming Superconducting RF (SCRF) gradients at 201 MHz ranging from 11 MV/m (already demonstrated [30]) to 17 MV/m.

Various acceleration schemes have been studied. Typically they begin with a linear "pre-accelerator" that accelerates the beam to about 1 GeV. The muons are then sufficiently relativistic to use a Recirculating Linear Accelerator (RLA) in which arc-sections return the muons to the same linac several times. Higher energies can be obtained using further RLAs and/or so-called FFAG (Fixed Field Alternating Gradient) accelerators. The ISS baseline scheme uses a new type of accelerator (a "non-scaling FFAG [31]") to raise the energy to 25 GeV. The EMMA [32] experiment at Daresbury has been designed to study non-scaling FFAG beam dynamics, which are interesting because the particles are accelerated out of the rf bucket. EMMA results will enable the attractiveness of this particular scheme to be better assessed.

After acceleration the interleaved $\mu^+$ and $\mu^-$ bunches are injected into the NF ring, where there circulate until they decay. Both racetrack (two straight sections) and triangular (three straight sections) geometries have been proposed. In principle both $\mu^+$

and $\mu^-$ bunches can be stored in a single ring, injected in opposite directions. However, in the ISS baseline design [22] there are two separate racetrack rings, one for each muon sign, with the beam-forming straight sections pointing to two distant detectors at different baselines.

## 5. MUON COLLIDERS: INTRODUCTION

Over the years $e^+e^-$ colliders, have played an important role in establishing and testing the Standard Model. The physics program that could be pursued by a new lepton collider ($e^+e^-$ or $\mu^+\mu^-$), with an energy $\sqrt{s}$ somewhere between 0.5 to a few TeV, has captured the imagination of the high energy physics community. With sufficient energy and luminosity this new accelerator would facilitate:

- understanding the mechanism behind mass generation and electroweak symmetry breaking;
- searching for, and perhaps discovering, supersymmetric particles and confirming their nature;
- hunting for signs of extra space-time dimensions and quantum gravity.

Within a few years results obtained from the Large Hardron Collider (LHC) at CERN are expected to more precisely establish the desired lepton collider energy, and whether the physics program can be begun with a lower energy ($\sqrt{s} \sim 0.5$ TeV) collider, or whether

we must go straight to multi-TeV energies to make contact with the physics. In either case, it is likely that multi-TeV lepton colliders will eventually be needed.

Both $e^+e^-$ and $\mu^+\mu^-$ colliders have been proposed as possible candidates for a multi-TeV lepton collider. However, a relativistic particle undergoing centripetal acceleration radiates at a rate proportional to the fourth power of the Lorentz factor ($\gamma^4$). This poses a challenge for multi-TeV $e^+e^-$ colliders, which cannot be circular, but must have a linear geometry and, with practical acceleration schemes, be tens of km long. Furthermore, beam-beam effects at the collision point induce the electrons and positrons to radiate, which broadens the colliding beam energy distributions. Since $(m_\mu/m_e)^4 = (207)^4 = 2\times10^9$, all of these radiation-related effects can be mitigated by using muons instead of electrons. A multi-TeV $\mu^+\mu^-$ collider can be circular and therefore have a compact geometry that will fit on existing accelerator sites. The expected footprints and beam energy spreads for multi-TeV $e^+e^-$ and $\mu^+\mu^-$ colliders are compared in Figs. 8 and 9 respectively.

Whichever high energy lepton collider is eventually built, it is important that the beam intensities are sufficient to probe very rare processes. Cross-sections ($\sigma$) for interesting processes at lepton colliders are often expressed in units of the QED point-like cross-section $R \equiv \sigma_{QED}\left(\mu^+\mu^- \to e^+e^-\right)$. The energy dependent $\sigma$ for representative Sandard Model processes at a MC are shown in Fig. 10 together with the relationship between $\sigma$, the event rate $r$, and the luminosity $L = r/\sigma$. Note that $\int L\ dt$ = $O(10^{34})$ cm$^{-2}$ s$^{-1}$ corresponds to 100 fb$^{-1}$ year$^{-1}$, and a multi-TeV MC with this luminosity could probe

processes with $\sigma$ down to $O$ (0.01$R$). The present MC luminosity design goals are for $L$ in the $10^{34}$ - $10^{35}$ cm$^{-2}$ s$^{-1}$ range.

## 6. MUON COLLIDER DESIGN and R&D

Muon Colliders with √s from 100 GeV to 4 TeV have been studied [5,33]. A MC facility is shown schematically in Fig. 1b. The front-end, up to and including the initial cooling channel, is similar (perhaps identical) to the corresponding NF front-end. However, in a NF the cooling channel must reduce the transverse emittances ($\varepsilon_x, \varepsilon_y$) by only factors of a few, whereas to produce the desired luminosity, a MC cooling channel must reduce the transverse emittances by factors of a few hundred and reduce the longitudinal emittance $\varepsilon_L$ by a factor $O$(10). Table 2 shows MC parameters corresponding to three representative schemes that are being studied. The different schemes correspond to different strategies for obtaining high luminosity, and different cooling technologies that result in different end-points in the 6D beam phase space. Following the cooling channel, the muons are accelerated to the energy of choice using circular accelerators and/or RLAs, and then injected into a ring so that $\mu^+$ and $\mu^-$ orbit in opposite directions and collide at one or more interaction points (IPs). To maximize the number of revolutions before the muons decay, the ring should be compact, and therefore use high field dipoles. For a given dipole field, since both ring circumference and muon lifetime are proportional to $E_\mu$, the number of revolutions before decay $N_{rev}$ is independent of $E_\mu$. In practice $N_{rev} \sim 1000$.

### 6.1 Cooling Channel

In the last couple of years self-consistent concepts have emerged for a complete MC cooling channel. There are several variants based on different technologies, and aiming at different end-points in 6D phase space. The path that the beam travels in ($\varepsilon_T, \varepsilon_L$)-space as it cools has been partially simulated. The result for one candidate scheme is shown in Fig. 11. Note that ionization cooling only reduces the transverse emittance. The longitudinal emittance is reduced by mixing the degrees of freedom as the beam cools. The design of the final cooling stages is particularly challenging. In the present schemes $\varepsilon_L$ is first over-cooled and then allowed to increase as the final ($\varepsilon_x, \varepsilon_y$) reduction takes place. All schemes considered so far require components with performances that are beyond the current state-of-art. In particular: (a) To continue the battle against scattering, the solenoid field at the end of the cooling channel must be very high. The highest practical field for the last few solenoids has yet to be established, but fields up to ~50T have been considered. The final MC luminosity is proportional to this field; (b) The mixing of transverse and longitudinal degrees of freedom is accomplished using solenoids "twisted" into a helix, and rf cavities must somehow be integrated into the design; (c) RF operation in the appropriate magnetic field configuration must be better understood and demonstrated.

### 6.2 Detector Backgrounds

A MC detector is imagined to be conceptually similar to detectors at other colliders (vertex detector, tracker, calorimeters, and muon detectors, with the vertex detector and tracker within a solenoid magnet). These detectors must operate in the presence of

various backgrounds. Unique to a MC are backgrounds that originate from muon decay. For example, a $\sqrt{s}$=4 TeV MC with one bunch containing $O(10^{12})$ muons would create $O(10^5)$ decay electrons per meter with a mean energy of 700 GeV. This sounds horrendous, but in the late 1990s detailed simulations showed [5] that with a carefully designed final focus system the backgrounds could be reduced so that a MC with $L=10^{35}$ $cm^{-2}s^{-1}$ would have detector background rates comparable to the those at the LHC with $L=10^{34}$ $cm^{-2}s^{-1}$. This is possible because the decay electrons born within a few meters of the IP remain within the beampipe in the region of the detector. In the final focus design studied, there was a 130m long straight section on either side of the IP and the last 6.5m was used to shield backgrounds. The shielding occupied cones with cone angles of $20^o$. Simulations predicted that most of the decay electrons (62%) interact upstream of the shielding, 32% interact in the shielding, and 10% pass through the IP without interacting. As the decay electrons respond to the fields of the final focus system, before they leave the beampipe they lose 20% of their energy by radiating on average 500 synchrotron photons with a mean energy of ~500 MeV. The resulting detector backgrounds have been simulated using two different programs which yield consistent results. Figure 12 shows the calculated particle fluxes. These fluxes can be used to estimate detector hit rates. For example, consider a cylindrical silicon vertex detector layer at a radius of 10cm. The simulations predict that in $1cm^2$ there with be 750 photons + 110 neutrons + 1.3 charged tracks. These particles yield 2.3 + 0.1 + 1.3 = 4.4 hits $cm^{-2}$. With 300 x 300 $\mu m^2$ pixels this yields an occupancy of 1.3%, which is considered acceptable. The occupancy can be further reduced, by a factor of ~100, by arranging the detector geometry and design so

that only coincidences between closely spaced pairs of hits that point back to the IP are read out [34].

### 6.3 Neutrino Radiation

Any straight section within the collider ring will produce a beam of muon decay neutrinos in the direction of the straight section. These neutrinos will exit the Earth at some point, perhaps a few tens of km away if the ring is deep. At the exit point, neutrino interactions in the rock create radiation at the surface. The radiation level increases rapidly with stored muon energy (note: flux $\propto E_\mu^2$, cross-section $\propto E_\mu$, energy in shower $\propto E_\mu$). Neutrino radiation from the IP straight sections is not considered a problem since those specific exit points can be fenced off. The real limitation is from the many short straight sections between magnets. Assuming $L = 10^{35}\text{cm}^{-2}\text{s}^{-1}$, the √s at which the neutrino radiation related dose from these short straights begins to be a potential problem is ~4 TeV. It is probably possible to push to higher energies by locating the ring at great depth, wobbling the beam orbit (to spread the neutrinos around), and making sure short straight sections point in benign directions.

In addition to MC design studies, component R&D is also proceeding. Indeed, much of the R&D discussed in the NF section can equally be considered as MC R&D (e.g. MERIT, MICE, EMMA). However, additional MC component development and testing is required. This MC specific R&D has so far been primarily a U.S. activity and has been rather limited in scope. However, in 2006 the Muon Collider Task Force (MCTF [35]) was established at Fermilab to complement the NFMCC R&D. The MCTF activities have

begun to explore 6D cooling channel options, including both “helical solenoid” and rf options. In particular, a so-called “HCC” 6D cooling channel option has been proposed [36] in which the helical channel, including the rf cavities, is filled with hydrogen gas at high pressure. The MCTF has begun to explore the viability of this option by preparing a beam test of high pressure hydrogen filled rf cavities, and building and testing a 4-coil model of the HCC. In addition the MCTF has begun studying the viability of an HTS option for the highest field solenoids at the end of the cooling channel.

## 7. OUTLOOK

Aspired timelines for completing the R&D and building a NF and a MC are illustrated in Fig. 13. The next NF step, which has begun, is the so called International Design Study (IDS) which hopes to deliver a “Reference Design Report” by 2012. By this time it is anticipated that all of the proof-of-principle tests will be completed and a NF could then become part of the particle physics “road map”. If the community wishes to proceed, after a few years of additional R&D, it is plausible that construction could start as early as the late 2010’s.

Muon Collider specific R&D is less advanced. The NFMCC and MCTF have recently proposed a joint R&D plan for the next 5 years which includes participation in the IDS and ongoing NF R&D, but is dominated by an enhanced emphasis on MC R&D with the goal of delivering a “Design Feasibility Study” report. The study would include (i) an end-to-end MC simulation based on components that are either within the state-of-art or

could be expected to be developed within a few years, (ii) an evaluation of the MC performance and physics program, (iii) a first defensible cost estimate, and (iv) planning for the subsequent R&D that must be done before a MC could be built, including component development and proof-of-principle experiments. It is thought that, if the community wishes to go down this path, a MC construction start in the early to mid-2020s is plausible.

There are, of course, significant technical challenges that must be met if NFs and MCs are to become a reality. In particular, critical for both types of facility is to understand how to build high gradient rf cavities that operate within the magnetic fields needed for viable bunching, phase rotation, and cooling channels. Critical for MC viability is a better understanding of how to realize a complete 6D cooling channel followed by appropriate demonstrations of the required technologies. There are many other items on the critical list, but we can hope that, by ~2013, (i) a NF will look like a very real option, and (ii) the community will have sufficient information to judge the cost and performance of a multi-TeV MC, and understand the timescale for completing the R&D.

ACKNOWLEDGEMENTS

This work is supported at the Fermi National Accelerator Laboratory, which is operated by the Fermi Research Association, under contract No. DE-AC02-76CH03000 with the U.S. Department of Energy.

LITERATURE CITED

1. Budker G. Proc. 7th Int. Conf. on High Energy Accel. (Yerevan, 1969), p.33.

2. Skrinsky A, Parkhomchuk V. Sov. J. of Nucl. Physics 12 (1981) 3.

3. Neuffer D. Part. Accel. 14 (1983) 75.

4. See for example papers in Nucl. Instr. And Meth., A350 (1994).

5. Palmer R, Tollestrup A, Sessler A (Eds.) Fermilab-Conf-96/092.

6. Geer S. Phys. Rev. D57 (1998) 6989.

7. See for example Brunner J. CERN-PPE-97-038, Apr 1997.

8. Bilenky S, Pontecorvo B. Phys. Rep. 4 (1978) 225:261.

9. Geer S, Schellman H (Eds.) hep-ex/0008064.

10. Holtkamp N, Finley D (Eds.) Fermilab-Pub-00/108-E.

11. Autin B, Blondel A, Ellis J. CERN-99-02 ; DeRujula A, Gavela M, Hernandez P. Nucl. Phys. B547 (1999) 21.

12. Mori Y. J. Phys. G: Nucl. Part. Phys. 29 (2003) 1527:1536.

13. Blondel A, Nucl. Instrum. Methods A451 (2000) 131:137.

14. MINOS Technical Design Report, nuMI-L-337 TDR.

15. Geer S, Mena O, Pascoli S. Phys. Rev. D75, 093001 (2007); Bross A, Ellis M, Geer S, Mena O, Pascoli S. Phys. Rev. D77, 093012 (2008); Ankenbrandt C et al. FERMILAB-PUB-09-001-APC (2009).

16. Maki Z, Nakagawa M, Sakata S. Prog. Theor. Phys. 28 (1962) 870.

17. Bernstein R, Parke S. Phys. Rev. D 44, 2069 (1991).

18. See for example Huber P, Winter W. Phys. Rev. D68 (2003) 037301.

19. King S et al. (ISS Physics Working Group) arXiv:0712.4129v2, 2007.

20. Osaki S, Palmer R, Zisman M, Gallardo J (Eds.) BNL-52623.

21. Geer S, Zisman M. (Eds), e-Print: physics/0411123; Berg S et al. Phys. Rev. Special Topics-AB 9 (2006) 011001.

22. Berg S et al. (ISS Accelerator Working Group) arXiv:0802.4023v1, 2008.

23. Abe T et al. (ISS Detector Working Group) arXiv:0710.4947v1, 2007.

24. Kirk H et al. (MERIT Collab.) Proc. 2007 Part. Accel. Conf., pp. 646:648.

25. Yonehara K et al. Nucl. Phys B (Proc. Suppl.) 149 (2005) 286:288.

26. Palmer R et al. arXiv:0809.1633v1.

27. Neuffer D AIP CP 721, p. 407 (2004).

28. Neuffer D. Advanced Accel. Concepts, AIP Conf. Proc. 156, 201 (1987).

29. Sandstrom R. (MICE Collab.) AIP Conf. Proc. 981, 107 (2008).

30. Geng R et al. Proc. of the 2003 Part. Accel. Conf. 1309:1311.

31. See for example Johnstone C, Koscielniak S. Proc. of EPAC 2004, 800:802.

32. Berg J.S. (EMMA Collab.) AIP Conf. Proc. 981, 330 (2008).

33. Ankenbrandt C et al. (Muon Collider Collaboration), Phys Rev. ST Accel Beams 2, 081001 (1999).

34. Chapman J, Geer S. Proc. of the 1996 DPF/DPB Summer Study on New Directions for High Energy Physics, Snowmass, Colorado (1996) 480:481

35. Ankenbrandt C et al. (Muon Collider Task Force) Fermilab-TM-2399-APC,2007.

36. Derbenev Y, Johnson R. Phys. Rev. ST Accel. Beams 8, 041002 (2005).

Table 1: Annual number of $\nu_\mu$ charged current interactions in a 50 kT detector at a distance $L$ from a NF with stored muon energy $E_\mu$. Results from [9].

| $E_\mu$ (GeV) | $L$ (km) | | |
|---|---|---|---|
| | 732 | 2900 | 7300 |
| 10 | $1.4\times10^5$ | $9\times10^3$ | $1.4\times10^3$ |
| 20 | $1.2\times10^6$ | $7.4\times10^4$ | $1.1\times10^4$ |
| 30 | $1.8\times10^7$ | $1.1\times10^6$ | $1.9\times10^5$ |

Table 2: MC parameters for 3 representative √s=1.5 TeV designs that are under study. Designs for other center-of-mass energies ranging from 0.1 TeV to 4 TeV have also been studied.

| | | | |
|---|---|---|---|
| Luminosity ($10^{34}$ cm$^{-2}$ s$^{-1}$) | 3 | 1 | 1-2 |
| Ring Radius (m) | 361 | 500 | 500 |
| Number of IPs | 4 | 2 | 2 |
| $\beta^*$ (cm) | 0.5 | 1 | 1 |
| Bunch Length (cm) | 0.5 | 1 | 1 |
| Number of Bunches | 10 | 1 | 1 |
| Muons/bunch ($10^{11}$) | 1 | 20 | 11 |
| $\varepsilon_{TN}$ (μm) | 2 | 25 | 12 |
| $\sigma_E / E$ | 0.01 | 0.001 | 0.002 |
| $\varepsilon_{LN}$ (m) | 0.35 | 0.07 | 0.14 |
| Proton Driver rep. rate (Hz) | 65 | 13 | 40-60 |
| Proton Driver (8 GeV) beam power (MW) | 3.6 | 3.2 | 1.9-2.8 |

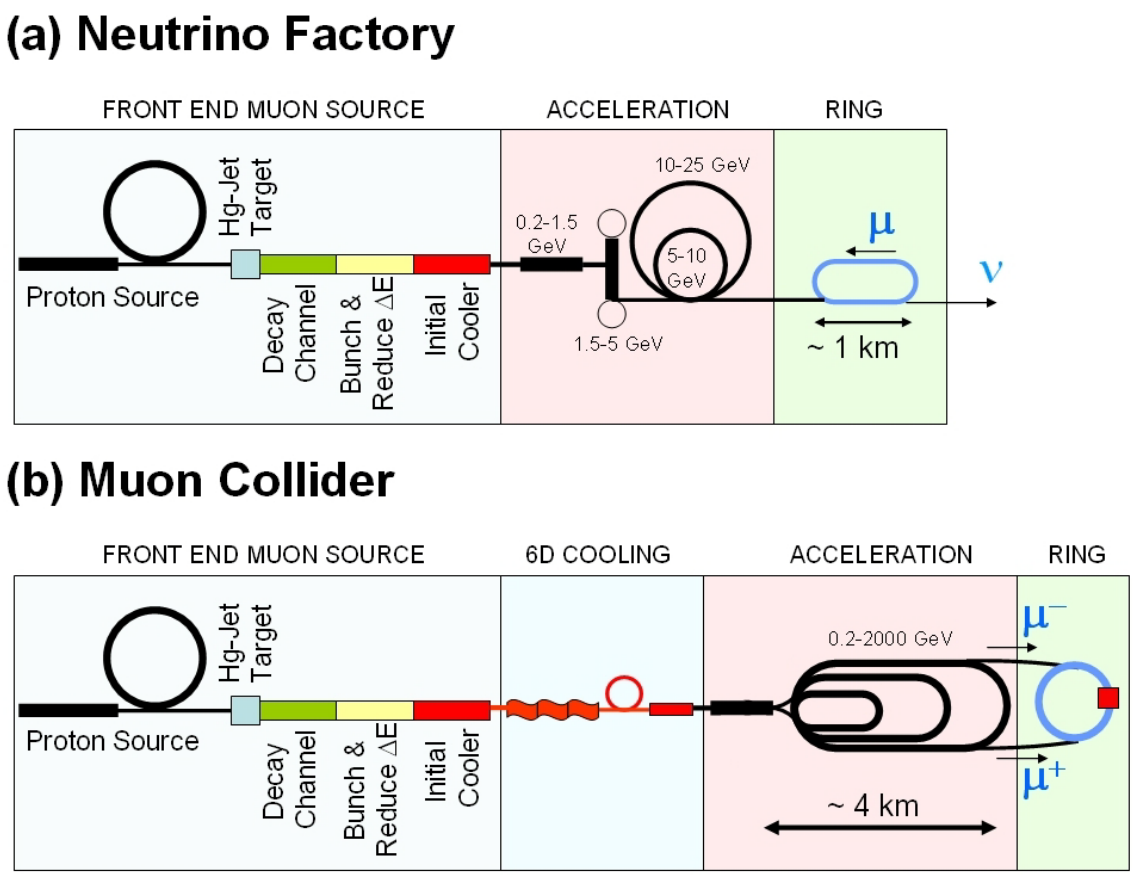


FIGURE 1: Schematics (not to scale) for (a) a 25 GeV Neutrino Factory and (b) a 4 TeV Muon Collider.

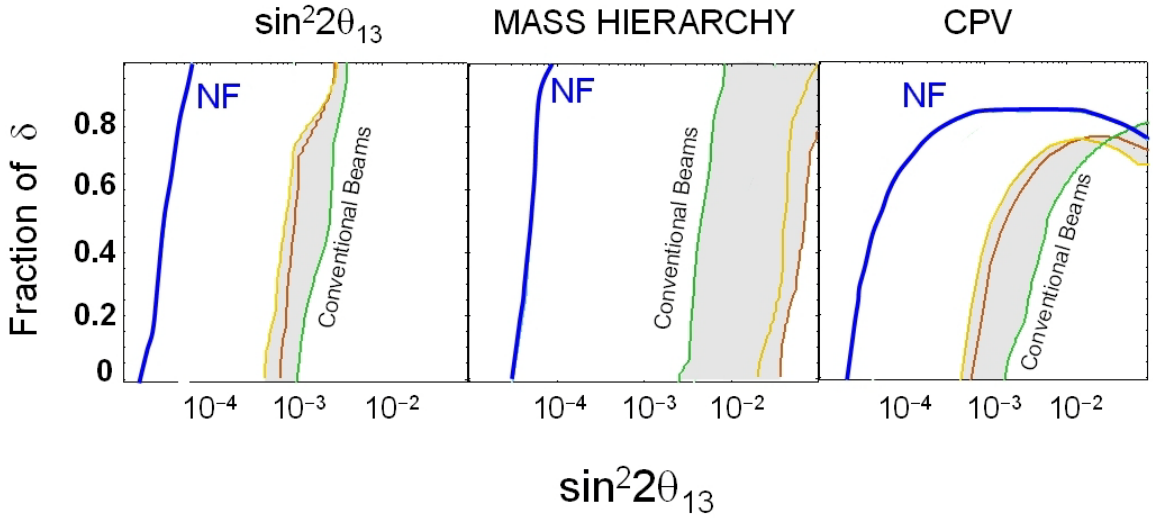


FIGURE 2: Results from the ISS [19]. As a function of $\sin^2 2\theta_{13}$, the fraction of all possible values of $\delta$ for which a discovery could be made at the 3σ level or better at a 25 GeV NF (blue curves) and for a selection of possible future conventional beam experiments (curves in gray bands).

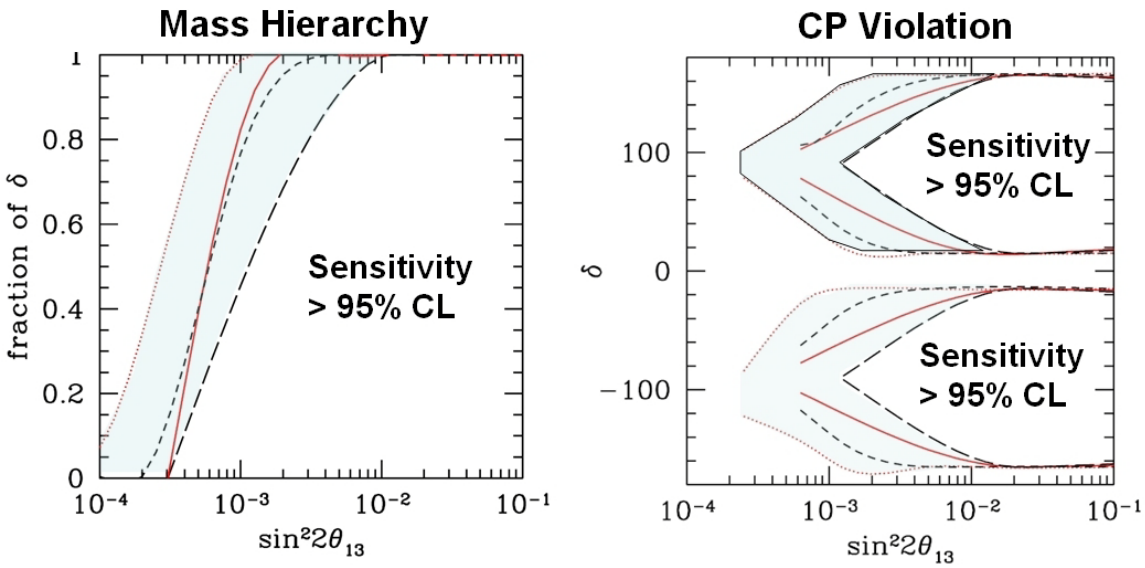


FIGURE 3: Sensitivity of a 4 GeV NF experiment [15]. As a function of $\sin^2 2\theta_{13}$, the fraction of all possible values of $\delta$ for which a discovery could be made at the 95% CL level or better at a long baseline experiment 1480 km from the NF. The different curves are for different assumptions about backgrounds and running time.

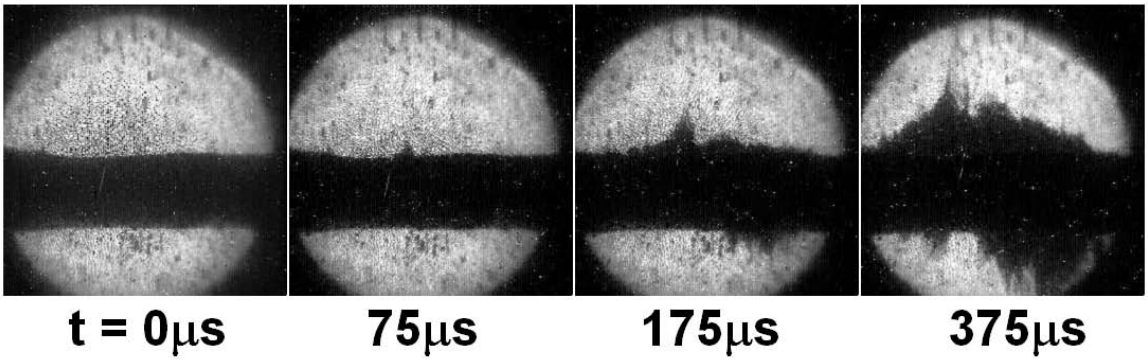


FIGURE 4: MERIT results. Sequential images of a Hg-jet target hit by a 24GeV beam pulse containing $10^{13}$ protons. The jet was within a 10T field (measurements have been made up to 15T). At longer timescales (~15ms) the jet re-establishes itself ready for the next proton pulse.

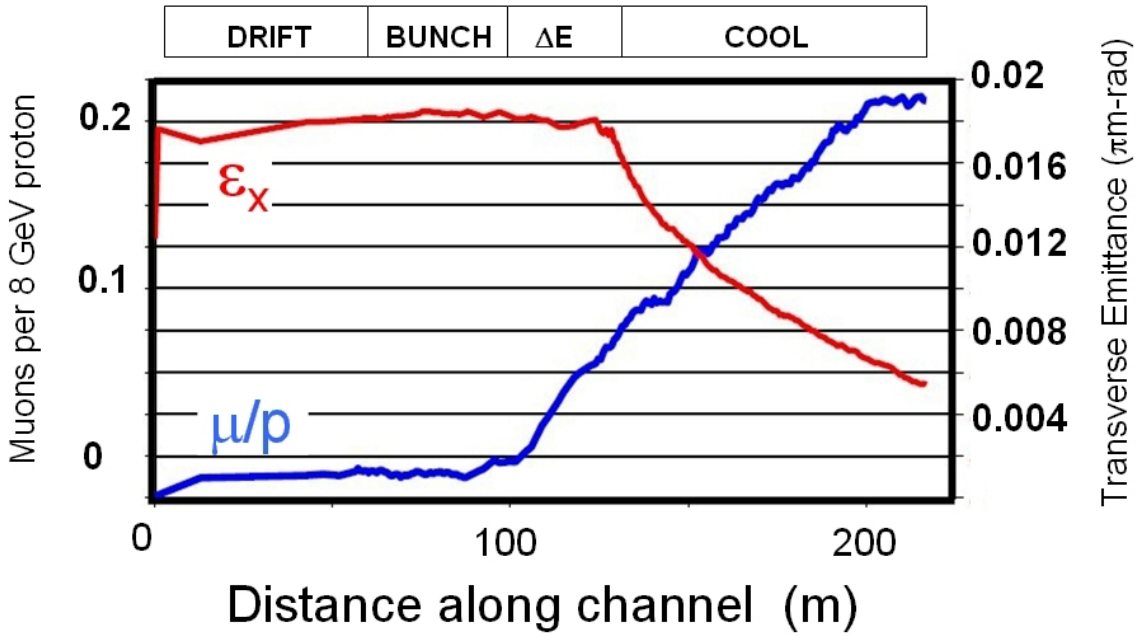


FIGURE 5: Front-end performance [15]. Simulated evolution within the channel of the transverse emittance (red curve) and the number of muons (per incident proton) that would fit within the acceptance of the initial acceleration stages (blue curve).

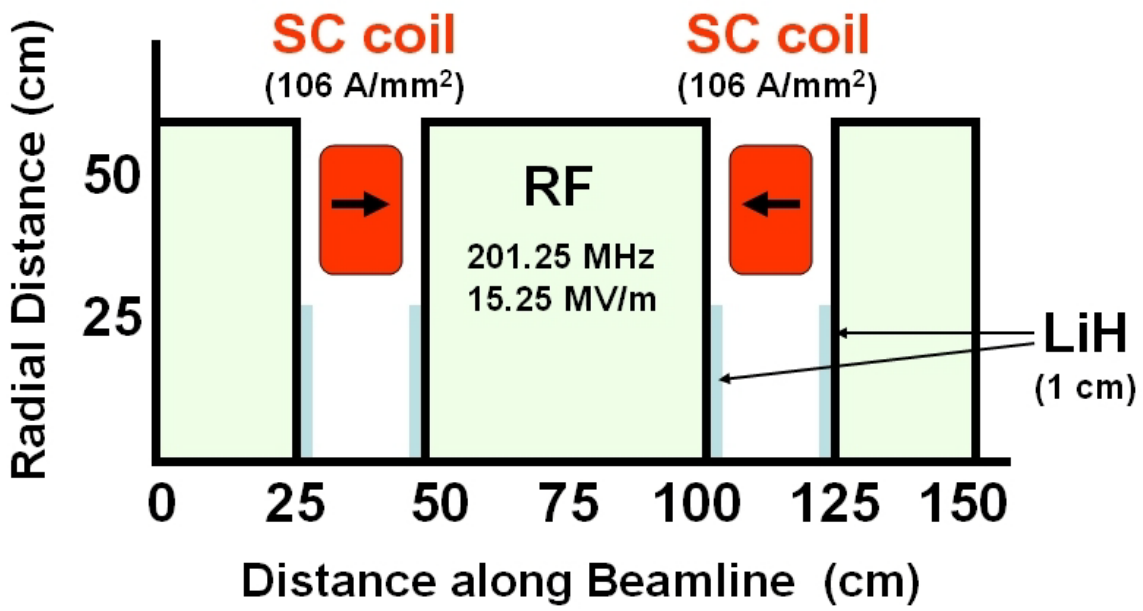


FIGURE 6: Cooling channel lattice [15]. Muons lose energy in LiH absorbers (blue), which is replaced by reaccelerating them in the longitudinal direction in rf cavities (green). The solenoids (red) confine the beam within the channel and radially focus the beam at the absorbers. Some representative component parameters are also shown.

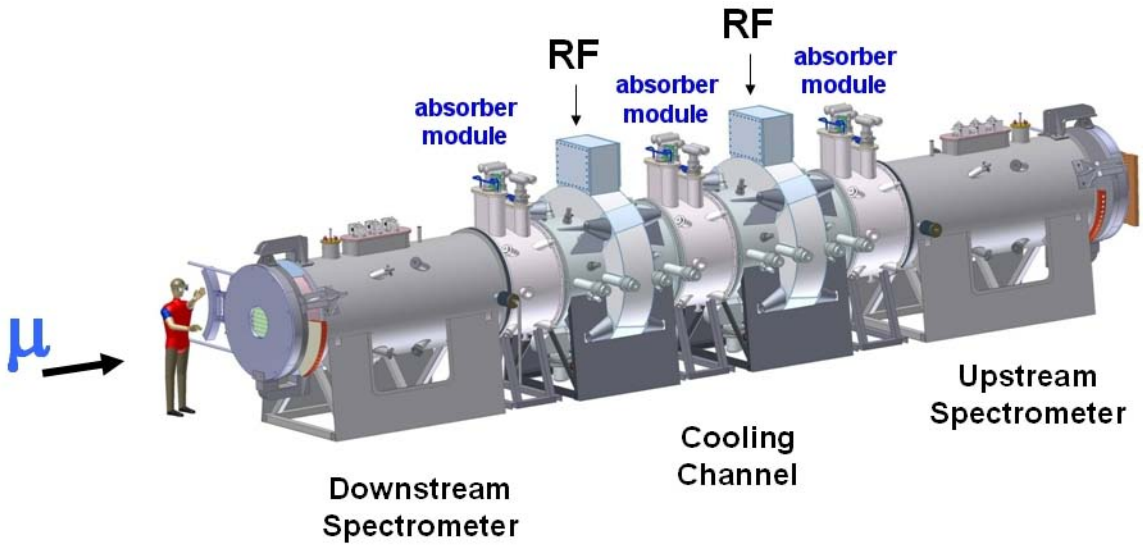


FIGURE 7: MICE setup. A short cooling channel section is sandwiched between upstream and downstream spectrometers that measure individual muons before and after "cooling".

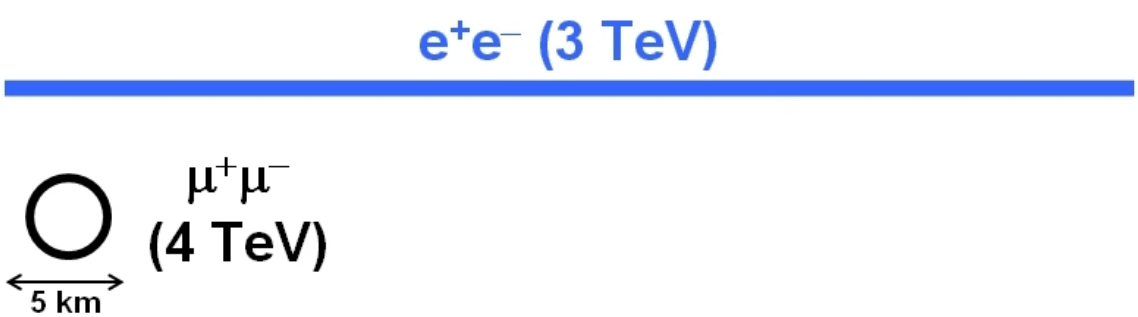


FIGURE 8: Comparison of high energy collider footprints. A 4 TeV muon collider would fit on existing accelerator laboratory sites.

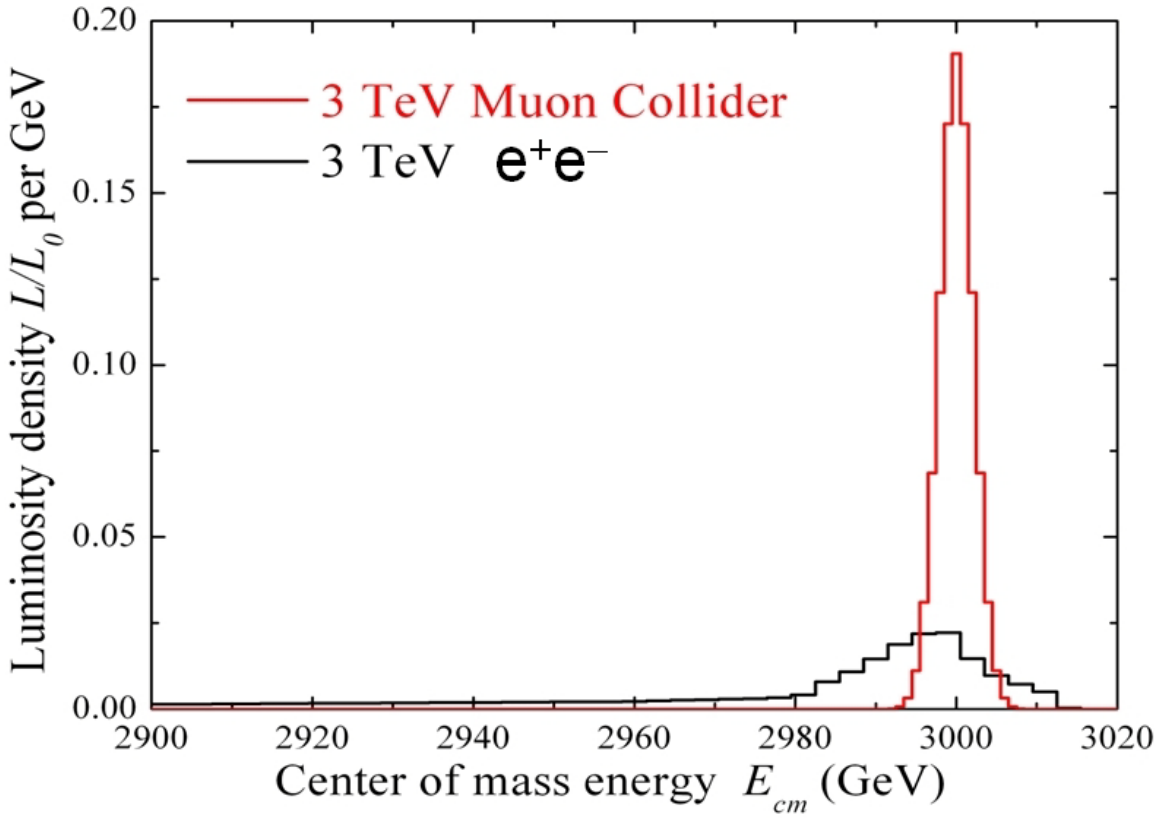


FIGURE 9: Comparison of the energy spreads for 3 TeV $\mu^+\mu^-$ and $e^+e^-$ Colliders.

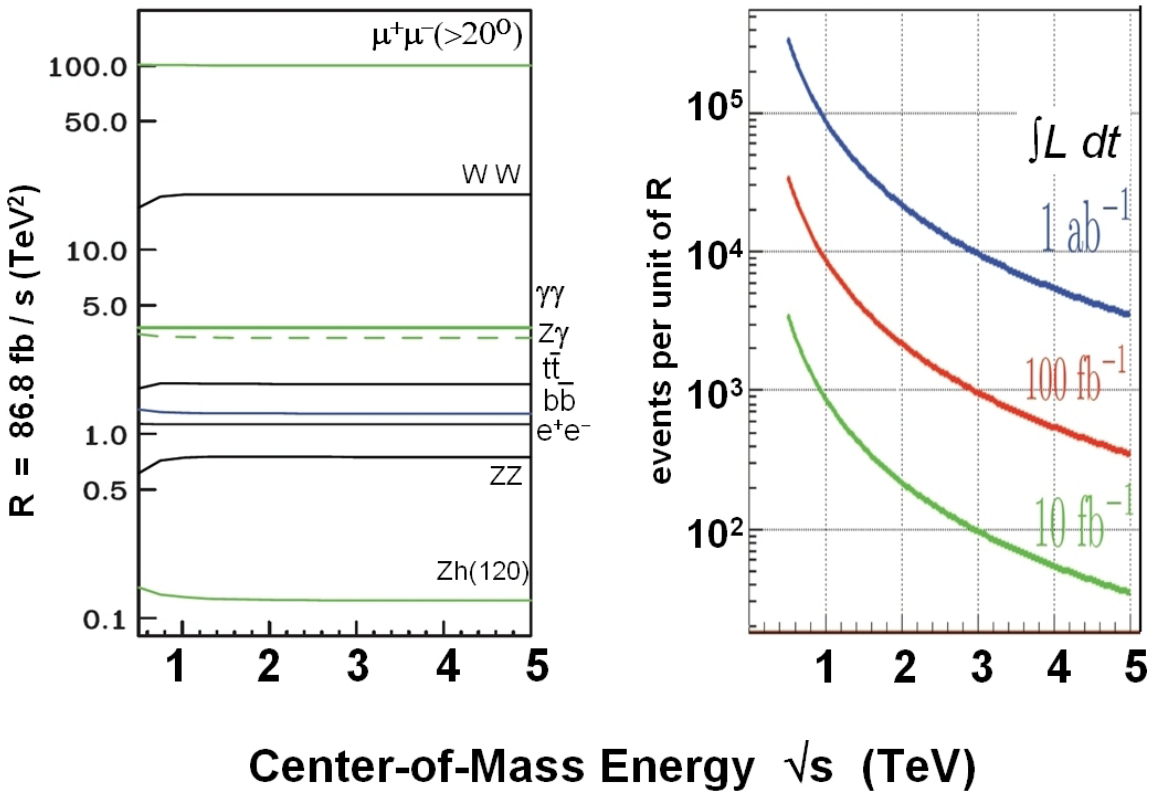


FIGURE 10: Dependence of MC event rates on luminosity. Energy dependent cross-sections (left plot) in units of *R* for various Standard Model processes ( $\mu^+\mu^- \to ab$ ) and, for three representative integrated luminosities, the total number of events for a σ=1*R* process (right plot).

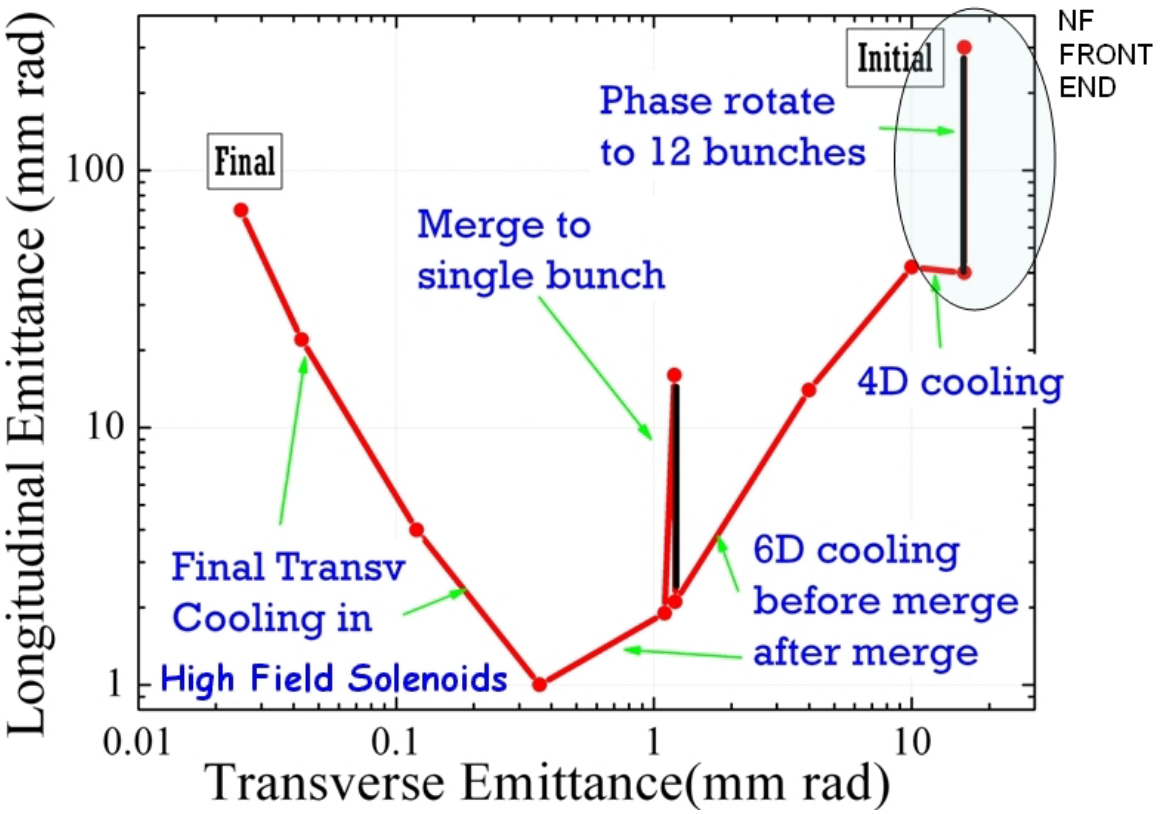


FIGURE 11: Simulated 6D cooling path corresponding to one particular candidate MC cooling channel. The first part of the scheme (indicated by the blue ellipse) is identical to the present baseline NF front-end.

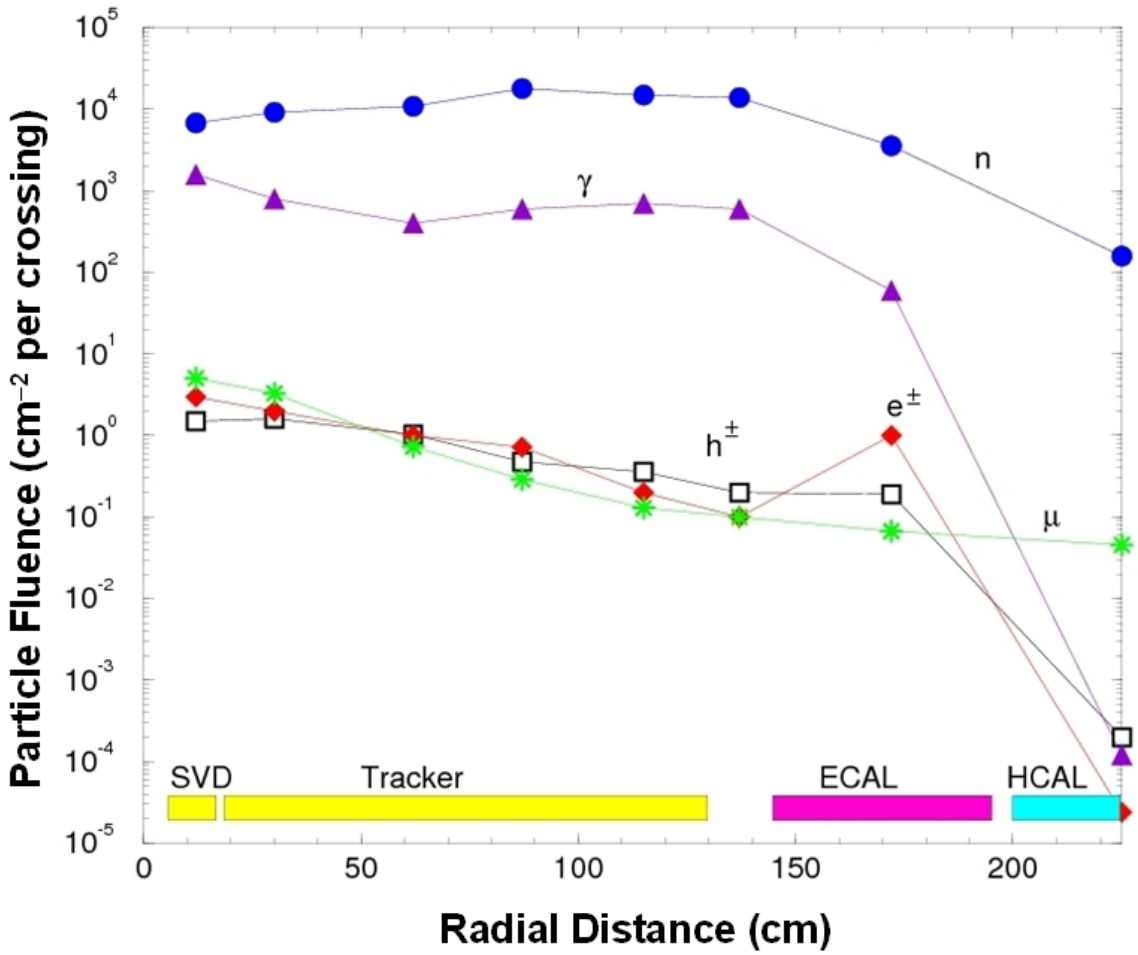


FIGURE 12: Calculated backgrounds at a 4 TeV Muon Collider [5]. Radial fluxes for various particle types, shown as a function of radius in the vicinity of the IP (±1.2m). Regions relevant for vertex detectors, main trackers, electromagnetic- and hadronic-calorimeters are indicated.

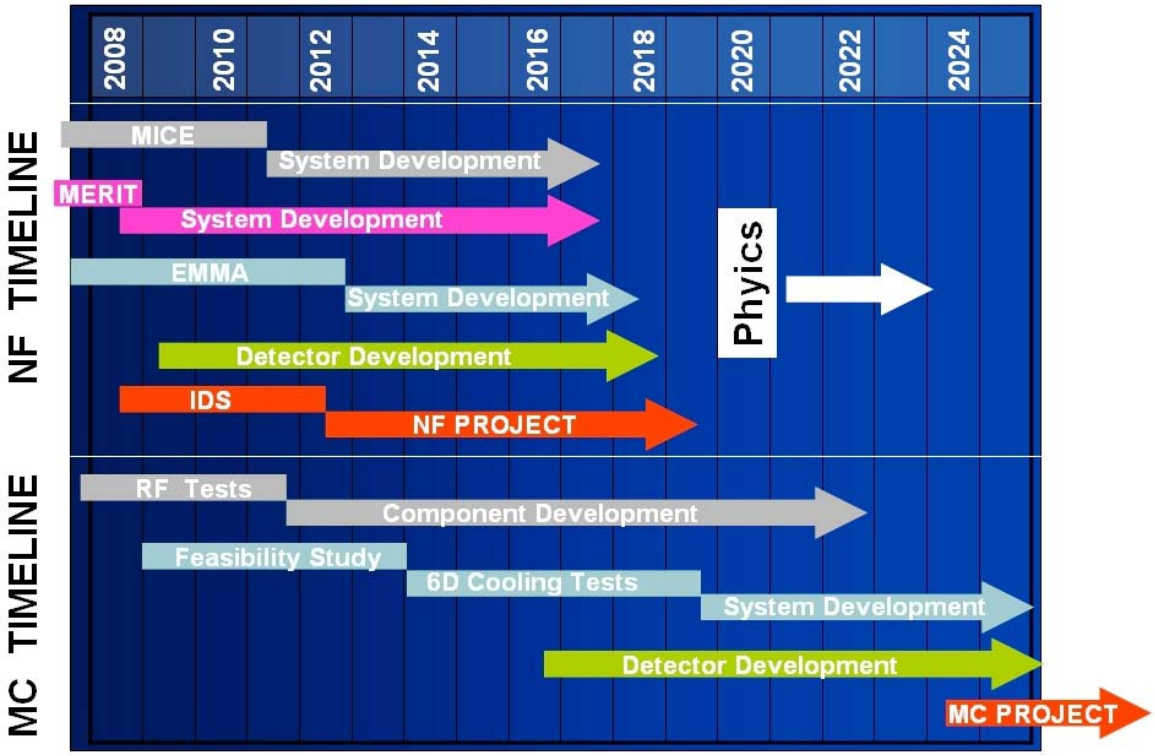


FGURE 13: Aspired timelines for NF (top half) and MC (bottom half) development. The NF timelines were established by the ISS.